W Morocco shortening during the Central Atlantic early post-rift

Fernández-Blanco, D.[1], Gouiza, M.[2], Klaver, J.[3], Brautigam, K.[4], Kluge, C.[1] and Bertotti, G.[1]

[1] TU Delft University, Faculty of Civil Engineering and Geosciences, Delft, Netherlands - corresponding author: Corresponding author contact data: Email geo.david.fernandez@gmail.com // OrcID 0000-0002-5326-9164 // Telf 0034 658 023314

[2] University of Leeds, School of Earth and Environment, Leeds, England, UK

[3] RWTH Aachen University, Structural Geology, Tectonics and Geomechanics, Aachen, Germany

[4] Vrije Universiteit Amsterdam, Tectonics and Structural Geology Department, Amsterdam, Netherlands

Abstract

The early post-rift phase of the Moroccan Atlantic margin is characterized by km-scale exhumation and erosion of its eastwards continental domains, coupled with an excessive subsidence seawards. We investigate the tectonic processes behind such Late Jurassic-Early Cretaceous crustal exhumation event, which remains unclear given that it took place significantly later than lithospheric breakup but prior to the Atlas/Alpine contraction. We study the Jbel Amsittene Anticline, which is ideally located on the coastal plain of the Atlantic rifted margin of Morocco and classically considered to develop by Late Cretaceous halokinesis and Neogene Atlas contraction. Our structural analysis indicates that this anticline is a fault propagation fold verging north that formed by active tectonics during Atlantic post-rift times, with a Triassic salt acting as a detachment plane. The anticline grew by NNW-SSE to NNE-SSW shortening as indicated by syn-tectonic wedges, regional kinematic indicators and structures in the Upper Jurassic to Lower Cretaceous rocks. It was further deformed and tightened during the Cenozoic, presumably in relation to the Atlas/Alpine contraction, as shown by km-scale tête-plongeante geometry at the axis of the anticline. Contrarily to observations in other sites of the Moroccan Atlantic margin, this paper favours a "tectonics-drives-salt" over a "salt-drives-tectonics" model, and points to factors other than small-cell mantle convection affecting the evolution of the rifted margin.

KEYWORDS: exhumation; W Africa; continental margin; shortening tectonics; Amsittene; anticline

1 Introduction

The evolution of the Atlantic rifted margin in Morocco is marked by a period of abnormal and excessive subsidence during the Late Jurassic-Early Cretaceous (Gouiza 2011; Bertotti and Gouiza 2012). This early post-rift subsidence affected the distal deep basins, the continental shelf and the proximal coastal basins of the Atlantic margin, and was coeval with km-scale exhumation and erosion of large domains in the east (Gouiza et al., 2017; Ghorbal et al. 2008; Ghorbal 2009; Saddiqi et al. 2009; Oukassou et al. 2013; Leprêtre et al. 2015). The tectonics of the exhumation event are still unclear, as it took place 30 to 50 My after lithospheric breakup between Morocco and Nova Scotia (Klitgord and Schouten 1986; Sahabi et al. 2004) and prior to the Atlas/Alpine shortening, which gave rise to the Atlas and the Rif mountain belts (Frizon de Lamotte et al. 1991, 2008; Laville and Piqué 1992). Attempts to link the Late Jurassic-Early Cretaceous exhumation in the east to the coeval subsidence in the west have shown the existence of contemporaneous NE-SW to NNE-SSW shortening that might have driven both upward and downward vertical movements along the margin (Gouiza 2011; Bertotti and Gouiza 2012). Similarly to other passive continental margins, where comparable movements have been detected (Japsen and Chalmers 2000; Japsen et al. 2006, 2009; Peulvast et al. 2008; Bonow et al. 2009), these anomalous vertical movements must be driven by regional tectonic processes, yet unknown. In this contribution, we provide field evidences from the Essaouira Basin to shed light on these tectonic processes.

The Essaouira Basin is located on the coastal plain of the Atlantic rifted margin of Morocco, bounded to the E and NE by the exhumed Palaeozoic basement highs of Massif Ancien of Marrakech and the Jebilet, respectively. The Essaouira Basin is thus an ideal location to investigate the tectonic processes responsible for the aforementioned vertical movements (Fig. 1, Fig. 2). Most of the compressional structures observed in the Essaouira Basin are attributed to the Alpine shortening events leading to the uplift of the Atlas Belt (Hafid et al. 2006; Hafid 2000; Ellouz et al. 2003). Thickness changes observed in Upper Jurassic to Upper Cretaceous rocks are interpreted as resulting from synsedimentary halokinesis (Hafid et al. 2006; Hafid 2000). However, recent studies show that many contractional structures developed during the Late Jurassic-

Early Cretaceous in the western High Atlas and surroundings (Gouiza 2011; Bertotti and Gouiza 2012; Benvenuti et al. 2017). The Jbel Amsittene Anticline, located in the central western part of the Essaouira Basin, is one of several comparable structures within the western Moroccan basins thought to be formed by salt diapirism from the Late Cretaceous onwards (Piqué et al. 1998; Hafid 2000; Le Roy and Piqué 2001). In this work, we carry out a structural analysis of the Jbel Amsittene based on field observations and structural modeling to investigate the tectonics of its formation and its relationship with the regional vertical movements recorded along the Atlantic margin.

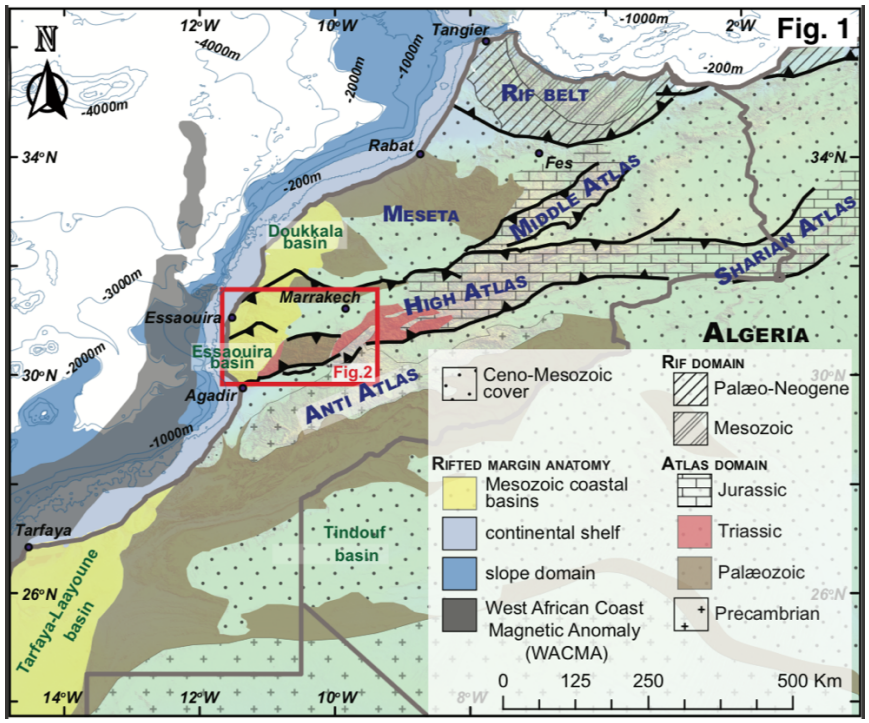

Fig. 1. Major tectono-sedimentary provinces of Western Morocco with the main Atlantic basins, modified after Gouiza 2011.

2 Geological background

The Essaouira Basin forms the western termination of the Moroccan High Atlas. It evolved as part of the Atlantic rift during Triassic to Early Jurassic times and as a proximal shallow-water platform of the Atlantic rifted margin since the Middle Jurassic (e.g., Hafid 2000). Later, during the Late Cretaceous to present-day convergence between Africa and Iberia/Europe, the Essaouira Basin in particular and the Atlas rift in

general, experienced a N-S to NNW-SSE shortening and inversion leading to the build-up of the Atlas Mountains (e.g., Hafid et al. 2006; Hafid 2000; Piqué et al. 2002).

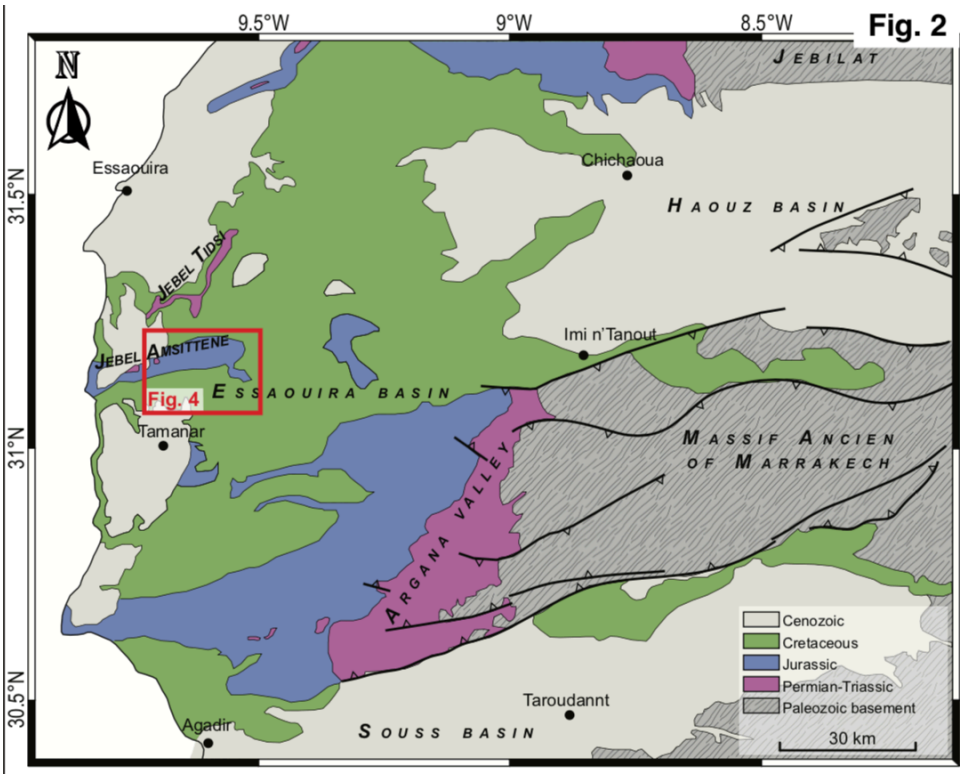

Fig. 2. Geological map of the western High Atlas (inverted Agadir continental margin basin), the southern part of the Essaouira Basin and the northern part of the Souss Basin. Simplified after Jadi, Bencheqroun, and Diouri (1970a,b), Ouzzani, Eyssautier, Marcais, Choubert and Fallot (1956), and Saadi (1982). From R. Zuhlke et al, 2004.

The extensional rift structures in the Essaouira Basin are grabens and half-grabens bounded by N-S to NNE-SSW normal faults and E-W transform faults (Hafid et al. 2006; Hafid 2000). These structures are filled by terrigenous red beds of Triassic age, unconformably overlain by an early Lower Jurassic evaporitic sag basin with widespread intercalations of basalt flows (Hafid et al. 2006). An early Pliensbachian unconformity, which is commonly considered to be the breakup unconformity, seals syn-rift sequences and structures (Medina 1995). Following continental breakup in the Central Atlantic, sedimentation became mostly marine in the Essaouira Basin, leading to deposition of the Middle Jurassic to Lower Cretaceous

thick carbonate platform, with sandstone and shale interbeds, and the Upper Cretaceous to Neogene shale-dominated series, with intercalations of limestone beds (Hafid 2000). The shortening in the Atlas domain, which initiated in the Late Cretaceous and led to the formation of the Atlas fold-and-thrust belt (Frizon de Lamotte et al. 2000; Piqué et al. 2002; Teixell et al. 2003), is also believed to form salt-cored anticlines in the Essaouira Basin, with minor inversion of Triassic normal faults (Hafid et al. 2006).

The inversion and uplift of the Atlas belt is not the only major tectonic event that affected the Moroccan margin after the opening of the Central Atlantic Ocean. Analyses of low-temperature thermochronology document a major exhumation event that affected most of the Precambrian-Palaeozoic domains exposed to the east of the Atlantic margin (i.e. Meseta plateau, Jebilet, Massif Ancien of Marrakech, Anti-Atlas belt) during Late Jurassic-Early Cretaceous times (Ghorbal et al. 2008; Ghorbal 2009; Saddiqi et al. 2009; Ruiz et al. 2011; Oukassou et al. 2013; Sehrt 2014). The Palaeozoic basement highs bounding the Essaouira Basin, the Massif Ancien of Marrakech to the east and the Jebilet to the northeast, experienced km-scale exhumation during the Late Jurassic-Early Cretaceous (Ghorbal 2009; Saddiqi et al. 2009). Exhumation events are also documented along the margin in the Meseta plateau to the north (Ghorbal 2009; Saddiqi et al. 2009) and in the Anti-Atlas to the south (Malusà et al. 2007; Ruiz et al. 2011; Oukassou et al. 2013; Sehrt 2014; Gouiza et al. 2017; Charton et al. 2018). Regional exhumation occurred during the post-rift stage of the Central Atlantic Ocean, i.e. 30 to 50 Myr after lithospheric breakup between Morocco and Nova Scotia (Klitgord and Schouten 1986; Sahabi et al. 2004), and before the Atlas/Alpine contraction that gave rise to the Atlas and the Rif mountain belts (Frizon de Lamotte et al. 1991, 2008; Laville and Piqué 1992).

3 Fieldwork observations from Jbel Amsittene Anticline

Jbel Amsittene is a well-exposed salt-cored anticline that strikes ENE-WSW. It is located on the coastal plain of the W Moroccan Atlantic margin, in the northwest of the Essaouira Basin between the cities of Essaouira to the north and Agadir to the south (Figs 1 and 2).

The stratigraphy of Jbel Amssittene used in this study is based on Duffaud et al. (1966), Jaïdi et al, (1970) and Zühlke et al. (2004). The stratigraphic column shown in Fig. 3 is taken from the 1:100000 Geologic Map of the study area (Jaïdi et al. 1970), and shows an almost-continuous series of Upper Triassic to Lower Cretaceous rocks unconformably covered by Quaternary sediments in areas near the coast. The oldest formation, exposed in the core of the anticline, comprises Upper Triassic (T) terrigenous sandstones and evaporites. A stratigraphic gap marks an erosional event that occurred before the deposition of open marine rocks during the Early Jurassic (J0-J1). A gradual transition from floodplain to inner shelf environment, during the Middle Jurassic (J2-J3), resulted in a sedimentary change from predominantly siliciclastic sand to shallow marine carbonate. The Upper Jurassic (J4-J5) sediments are mainly shallow marine carbonates of inner shelf to lagoonal environment, although there remains some siliciclastic input. A change from inner shelf (J/C-C1-C2) to outer shelf environment occurred by the end of the Early Cretaceous (C3). Quaternary terrestrial colluviums and coastal deposits overlie the Mesozoic deposits (Fig. 3).

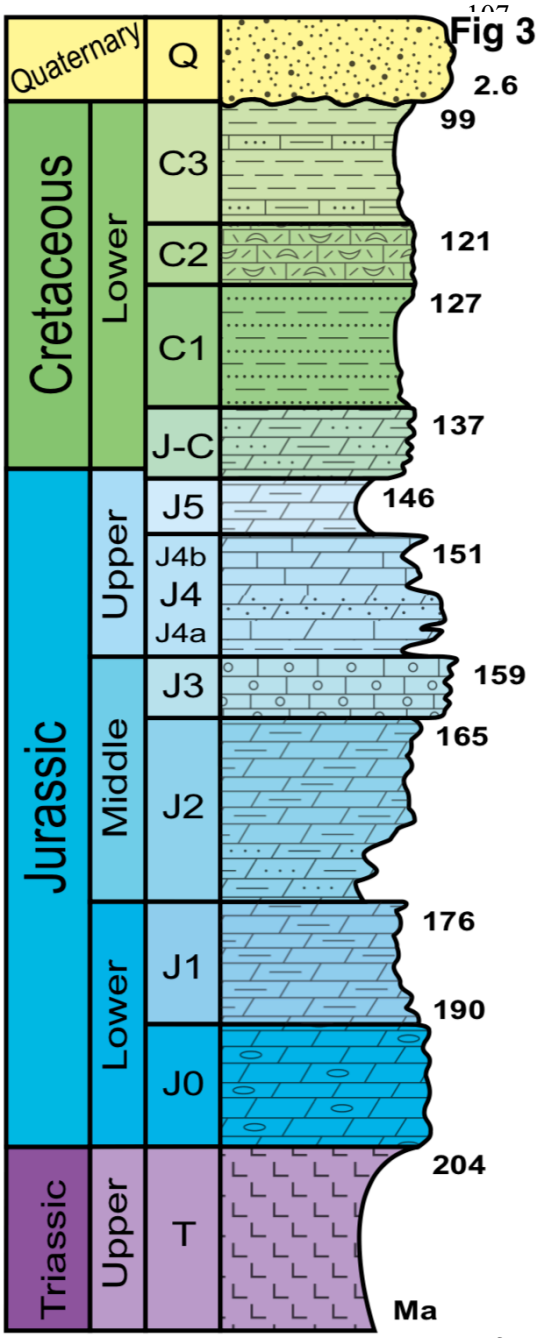

Fig. 3. Simplified chronostratigraphic and environmental column of the Jbel Amsittene area. Based on Hafid (2000), the Geological map of Tamanar from the Moroccan Geological Survey and Zlke et al. (2004).

To understand the tectonic history of the Jbel Amsittene Anticline, we performed a detailed structural fieldwork. Whenever possible, we have differentiated strain involving soft sediments depositing during the early post-rift of the Central Atlantic providing key information on the stress field during growth of the structures, especially in the Late Jurassic - Early Cretaceous, from observations of strain providing stress orientations of Alpine events, presumably in the Cenozoic. We show relevant and representative outcrops (Fig. 4) that summarize the main structural observations along three cross-sections.

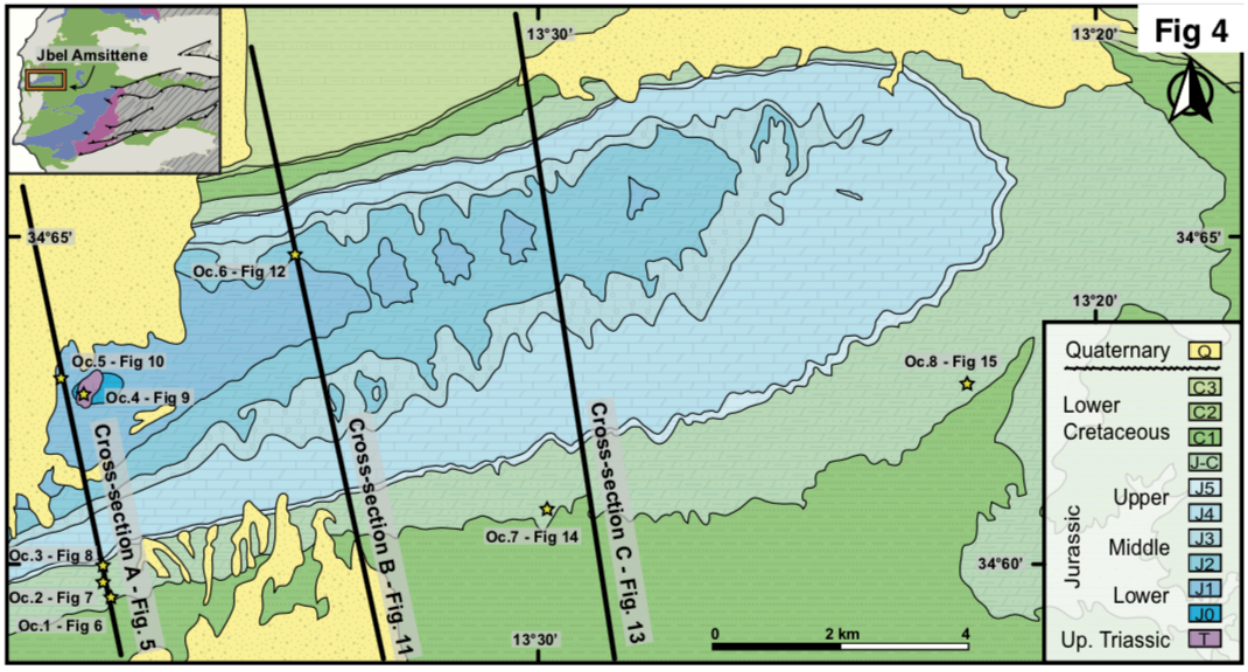

Fig. 4. Geological map of the Jbel Amsittene Anticline, showing the location of the main observations in the field and derived cross-sections that have been used to constrain the geological evolution of the area.

The geological cross sections, located roughly 4 km apart, run NNW-SSE across the anticline axis and were constrained by bed measurements and field observations. Cross-section A (Fig. 5) runs parallel (NNW-SSE) to a road-cut for most of its length, which results in the best rock exposures in the area. Jurassic and Cretaceous rocks outcrop in the south and central parts of the profile and are covered by the quaternary deposits in the northern region. Cross-section B (Fig. 11) is located ~4 km east of cross-section A and runs parallel to it. Cross-section B is often covered by vegetation and has poor accessibility with a small number

of well-preserved outcrops. Cross-section C (Fig. 13) runs parallel to previous sections, and is located ~4 km east of cross-section B. We also describe two sections and an outcrop located farther east. Finally, we describe and recapitulate information relevant for the discussion in the form of along-strike and across-strike lateral variations, syn-sedimentary deformation, and a 3D thickness model.

3.1 Western profile: cross-section A

Lower Lower Cretaceous (C1) to lower Middle Jurassic (J2) layers dip south in most of the southern flank and change from horizontal to steeply north-dipping where the topography is the highest. North of the topographic high, layers dip south again and finally outcrop as overturned, prior to being covered by the Quaternary deposits in the northernmost area of the section. These outcropping Quaternary rocks prevent thickness comparison between most older units on both sides of the anticline, but those that could be compared show no thickness changes. The transition from horizontal to overturned layers is observed in the oldest Jurassic rocks exposed in this section (lowermost Jurassic, J1). The dip of the stratigraphic layers indicates a northward verging anticline with a tête-plongeante (plunging head) shape (sense Seguret 1972) in its central-northern sectors.

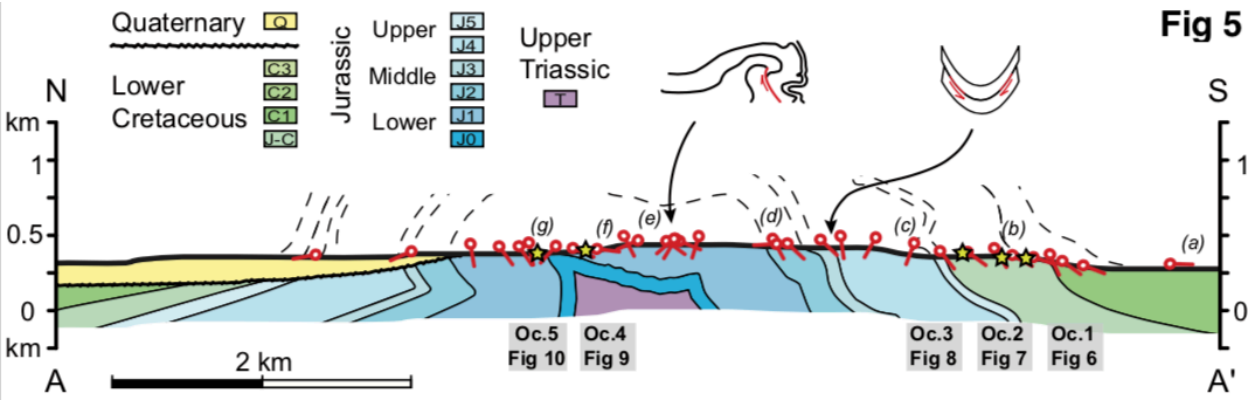

Fig. 5. Western profile: Cross-section A.

Lower Cretaceous rocks dip gently to the south (10˚-20˚) in the southernmost part of the southern flank ("a" in Fig. 5), and become steeper towards the north, reaching dips of ~80˚ at the highest point of the topography. Changes in dip are not constant and north dipping layers outcrop in the central sector of the southern flank (Fig. 5), within the middle and lower Upper Jurassic rocks (J4). Moving north, the dip of the layers locally changes in relation to secondary small-scale (tens of m) N-verging folds. In a local topographic flat (Fig. 5) there are three conjugate fault sets in the uppermost Upper Jurassic-lowermost Lower Cretaceous (J-C) limestones (Oc1; Fig. 6, Table I).

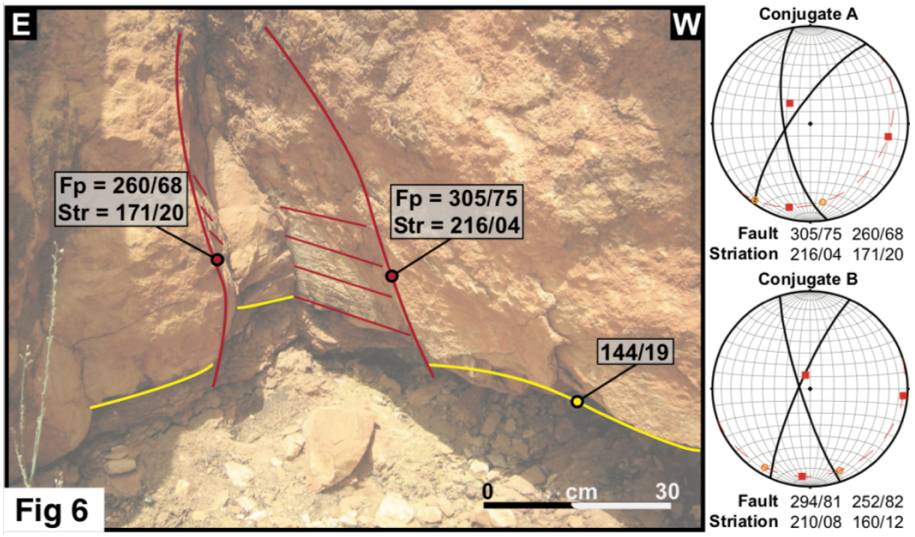

Fig. 6. Outcrop 1 (Oc.1). Conjugate sets and their stress directions, which indicate a north to south to north-northeast to south-southwest shortening.

Bedding	Present orientation			Orientation before tilting		
	σ_1	σ_2	σ_3	σ_1	σ_2	σ_3
144/19	010/09	256/68	103/20	014/22	208/67	106/02
144/19	183/01	282/81	093/09	005/13	171/76	274/03
146/28	203/28	344/56	103/18	195/11	031/79	286/03

Table I. Orientation of the main stresses derived from Out1 (Fig. 6).

The regional bedding dips gently to the SSE, and the three conjugate fault sets show clear striations of sub-horizontal to roughly S directions that we measure on the fault place as 216/04 and 171/20. The fault planes and associated striations are indicative of N-S to NNE-SSW maximum horizontal stresses in both non rotated rocks and rotated with respect to the regional bedding (to pre-tilt position). From this outcrop northwards, the strata dips start to increase and reach values up to ~55˚ toward the south ("b"; Fig. 5). Less than 50 m before the exposure of the lower Lower Cretaceous rocks (C1), a N-S-striking sub-vertical neptunian dyke of marine clastics cuts S-dipping strata (Oc2; Fig. 7). A few meters northwards, a syn-sedimentary N-verging ramp fold indicates soft sediment deformation (Oc3; Fig. 8). Whereas the conjugate fault sets in Oc.1 suggest no deformation took place before deposition of lowermost Lower Cretaceous – uppermost Upper Jurassic unit (J-C), the latter two synsedimentary structures (Oc2; Oc3) indicate NNW-SSE shortening during its deposition.

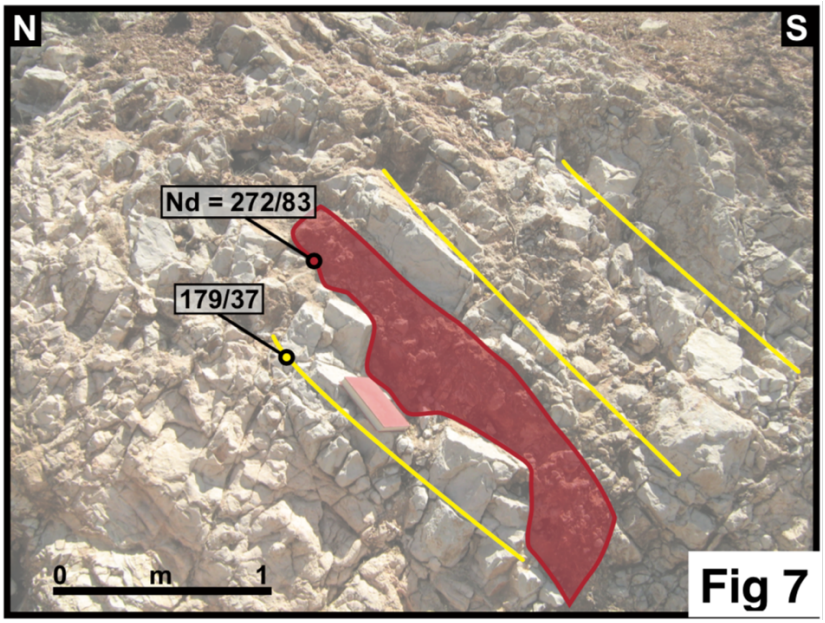

Fig. 7. Outcrop 2 (Oc.2). Neptunian dyke with a present position of 272/83. Assuming horizontal bedding at the moment of deposition, the neptunian dyke developed vertically, and suggests east-west extension.

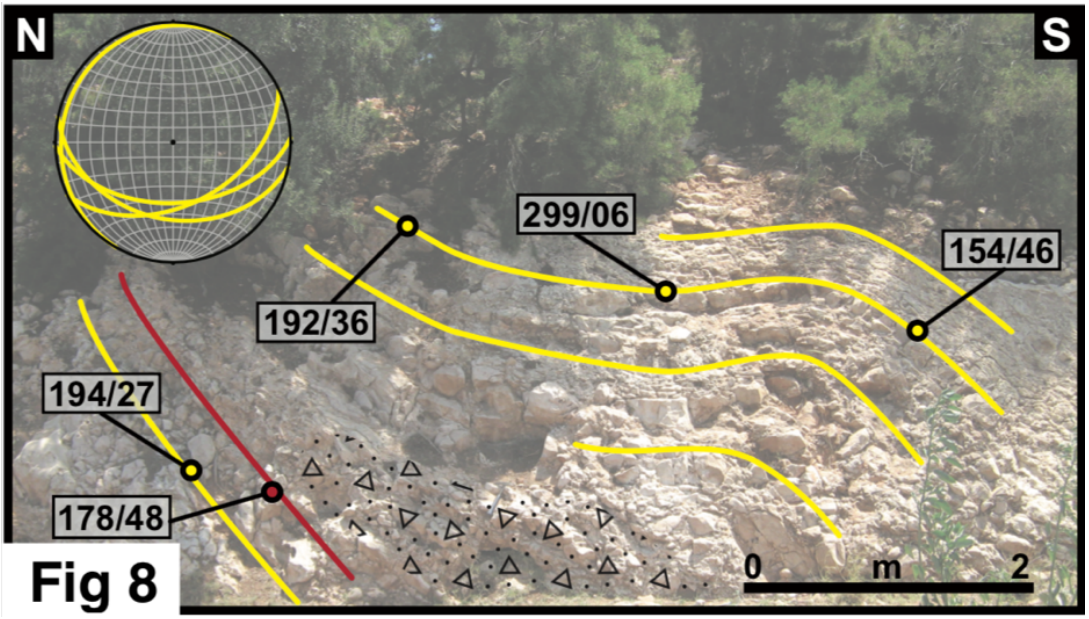

Fig. 8. Outcrop 3 (Oc.3). Folded and faulted soft sediments in a syn-sedimentary ramp fold, verging north, indicating shortening in a 160-340 direction during the 144-150 Ma (latest Jurassic).

Structures north of these outcrops seem to be exclusively related with the Alpine deformation phase. Approximately 200 m north of these outcrops, the Upper Jurassic layers (J5) are found dipping north ("c" in Fig. 5). For some 400 m, in the lower and middle Upper Jurassic rocks (J4), these steep and sub-vertical N-dipping overturned layers often alternate with areas of S dipping rocks with similar attitudes ("d"). Bedding-parallel flexural slip associated with Alpine deformation is common and related striations show a N-S slip direction. Northward, Middle Jurassic (J3-J2) strata dip consistently south until the highest topography of the profile is reached ("e"). North of the topographic high, the orientation of Lower Jurassic strata (J1) changes from subvertical (~80˚) to subhorizontal with a gentle S-dip within a distance of ca. 500 m (Fig. 5). Between the sub-vertical and sub-horizontal Lower Jurassic (J1) layers, S and N sub-vertical dipping strata alternate. Within this sector ("f" in Fig. 5), highly deformed structures appear, showing faulted and folded strata, m-folds, recumbent folds, fault-related-folds, and more complex features, with unclear or non-sequential vergence. More to the north the strike of the Lower Jurassic strata show no consistent trend for ~300 m, and outcrop as overturned (up to ~60˚) or S-dipping layers. At a similar latitude,

~300 m east off the section and roughly 5 km south of Smimou village, Upper Triassic evaporites (T) outcrop in a circular depression of approximately 1 km in diameter (Oc.4; Fig. 9). An intrusive contact is seen between the evaporites and the lowermost Jurassic unit (J1). The Lower Jurassic bedding dips away from the outcropping evaporites, from sub-vertical nearby to 25˚ farther away from them. The strike directions of these Jurassic rocks vary consistently around the salt, in an overall concentric configuration. The strike directions progressively change to the regional E−W to SW−NE trends 300-400 m away from the evaporites. Continuing north along the cross-section A, overturned strata become subvertical (80˚-85˚) ("g") and finally N-dipping, before reaching the discordant sub-horizontal Quaternary (Q) rocks that cover most of the northern flank. In this area, a sequence of SSE-verging fault-propagation folds (Oc.5; Fig. 10) outcrops in the Lower Jurassic (J1), with axial planes indicating a SSE-NNW shortening direction (Fig. 10).

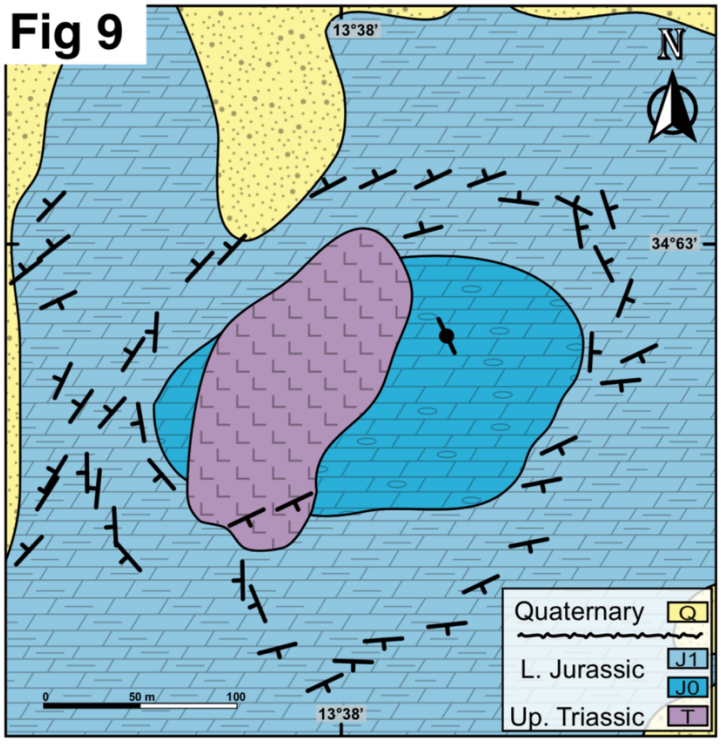

Fig. 9. Outcrop 4 (Oc.4). Map of the salt outcrop in the west and adjacent formations, showing the bedding strikes around the evaporitic body.

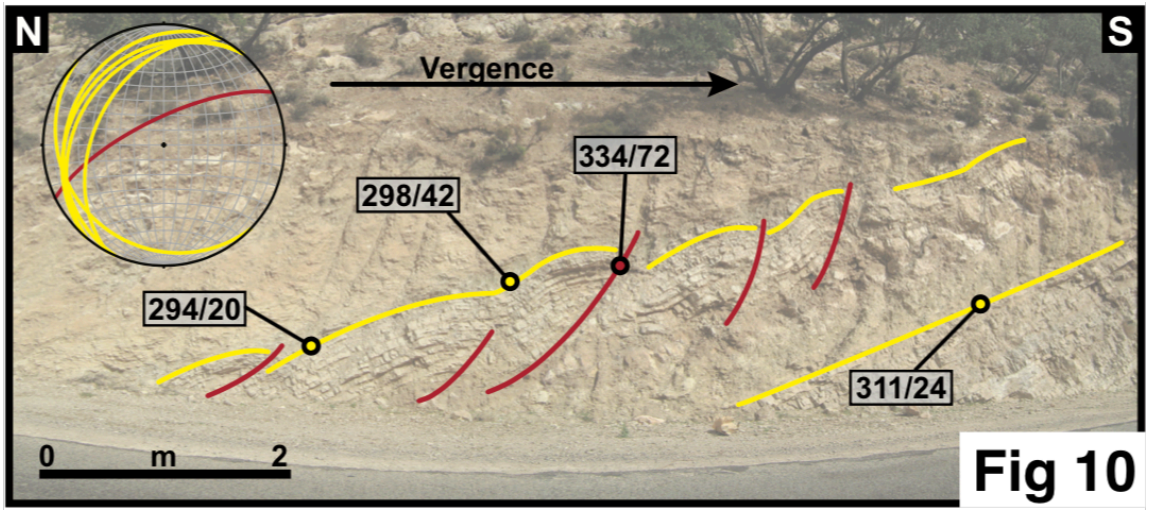

Fig. 10. Outcrop 5 (Oc.5). Reverse faults and folds with southeastern vergence, in outcrop situated less than 200 meters east of the outcropping salt (Fig. 9). Rocks in the outcrop are not affected by halokinesis, and show signs of compressional deformation. The orientation of the fault planes and the axial planes of the folds are similar and indicate NNW-SSE shortening.

3.2 Central profile: cross-section B

Gently south dipping lower Lower Cretaceous (C1) to lower Middle Jurassic (J2) layers outcrop from the southern side of the anticline until significantly north of the topographic high (Fig. 11). The oldest rocks seen in the section are Lower Jurassic (J1) and outcrop ~1,5 km north of the topographic high, in the core of the anticline. North of the hinge of the anticline there are steep north dipping layers of lower Middle Jurassic (J2) to Lower Cretaceous (C1) age. Some of these steep layers are overturned and dip south. Further north, the Lower Cretaceous strata (C2-C3) have gentle north dipping slopes. The uppermost Upper Jurassic to lower Lower Cretaceous (J-C to C1) rocks are significantly thinner in the northern (~350 m) than in the southern (>900 m) flank of the Jbel Amsittene (Fig. 11).

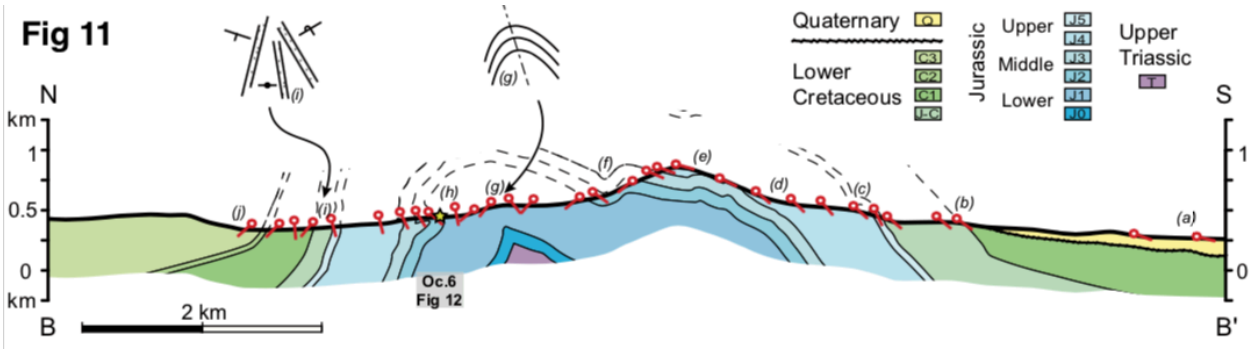

Fig. 11. Central profile: Cross-section B.

In the southernmost of cross-section B, Quaternary (Q) deposits cover Lower Cretaceous rocks (C1-C3) ("a" in Fig. 11). Northwards, the rocks of the uppermost Upper Jurassic to lower Lower Cretaceous (J-C to C1) outcrop with consistent dips of ~40° to the south ("b"). Upper Jurassic (J4-J5) layers have steeper dips that vary from ~40° to ~65° to the south ("c"). Moving north, the Middle Jurassic (J2-J3) layers gradually decrease in steepness from ~45° to ~35° to the south ("d") and become roughly parallel (10°-20° to the south) to the topography ("e") as they reach the topographic high.

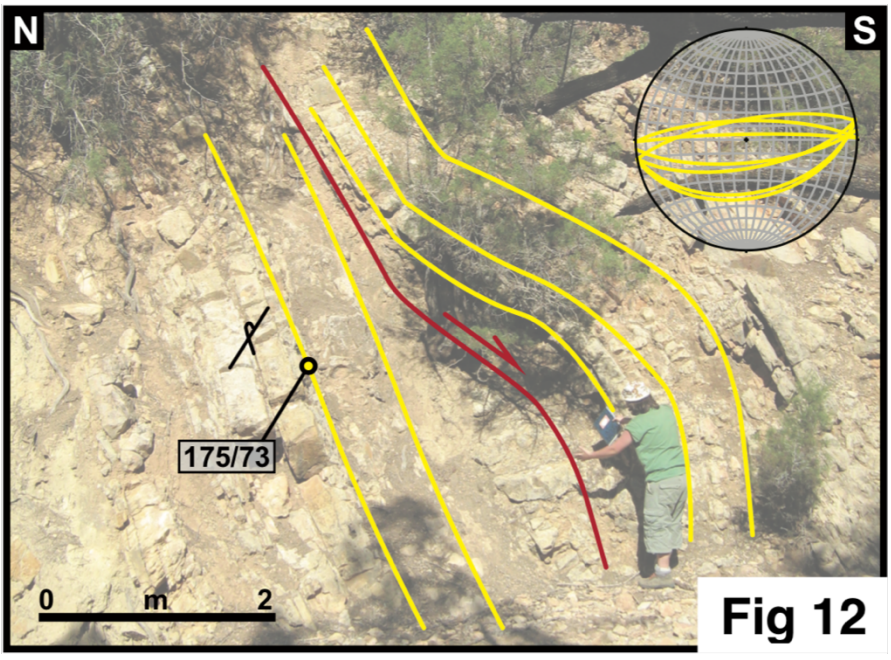

Fig. 12. Outcrop 6 (Oc.6). Underthrust in overturned strata, S_0 is 175/73. Fault-bend fold, with top to the south movement. The fold in the hanging wall has a fold axis of 085/06 and axial plane of 022/14.

241 Starting 300 m northwards of the topographic high, ~20° to 40° south dipping layers alternate with
242 ~40° north dipping layers. This trend continues for ~400 m, and is seen also for part of the Lower Jurassic
243 (J1) rocks ("f"). Layers are folded asymmetrically in this area until the northward dips become dominant
244 ("g" in Fig. 11). Advancing farther north, these Lower Jurassic (J1) layers overturn and dip south again, for
245 a distance of more than 900 m. Lower Middle Jurassic (J2) overturned layers outcrop showing the largest
246 overturn along this profile (175°/73°) ("h"). These Jurassic rocks are locally underthrusted in a fault-bend
247 fold structure that indicates top to the south motion (Oc.6; Fig. 12). The layers remain sub-vertical for
248 around 1100 m, and gradually decrease in steepness, from ~85° to ~50° to the north, in the lowermost
249 Cretaceous (J-C) unit ("i"). Toward the north, layers of the lowest Lower Cretaceous (C1) are sub-vertical
250 again, while the middle Lower Cretaceous (C2) strata have shallower dips (40° N) ("j") that decrease
251 gradually to 20° N when reaching the upper Lower Cretaceous (C3) rocks. Observations along the cross-
252 section B show no evidence of synsedimentary deformation in the uppermost Upper Jurassic to lower Lower
253 Cretaceous (J-C to C1) rocks but these units show a decrease of >500 m in thickness across the anticline
254 strike.

255 ### 3.3 Eastern profile: cross-section C

256 Cross-section C portrays a north vergent anticline with two hinges, showing a northern steep dipping flank
257 and a southern shallow dipping flank (Fig. 13). The rocks exposed along this easternmost section are early
258 Middle Jurassic (J2) to late Early Cretaceous (C3) of age. The thickness of the lowermost Cretaceous (J-C)
259 formation varies from approximately 550 m on the southern flank to 400 m on the northern flank of the
260 anticline, whereas the thicknesses of the Jurassic formations J2 to J5 are constant along the profile.

261 In cross-section C, the southern flank of the Jbel Amsittene Anticline is characterized in by south
262 dipping sedimentary beds ("a" in Fig. 13), with subhorizontal Cretaceous rocks in its southernmost sector.
263 Towards the north, older south-dipping rocks crop out. Within the lowermost Lower Cretaceous –
264 uppermost Lower Jurassic formation (J-C), layer inclinations vary between approximately 30° and 80° to

the south ("b"). Here, the layers are locally offset by cm to dm-scale reverse faults, which indicate N-S to NNE-SSW shortening coveal with sedimentation. Outcrop 7 (Oc. 7; Fig. 14) shows an example of these reverse faults. This SSW dipping fault has ~20 cm offset and terminates in the slumped overlying sediments that show soft deformation, indicating syn-sedimentary deformation during the early post-rift of the Central Atlantic.

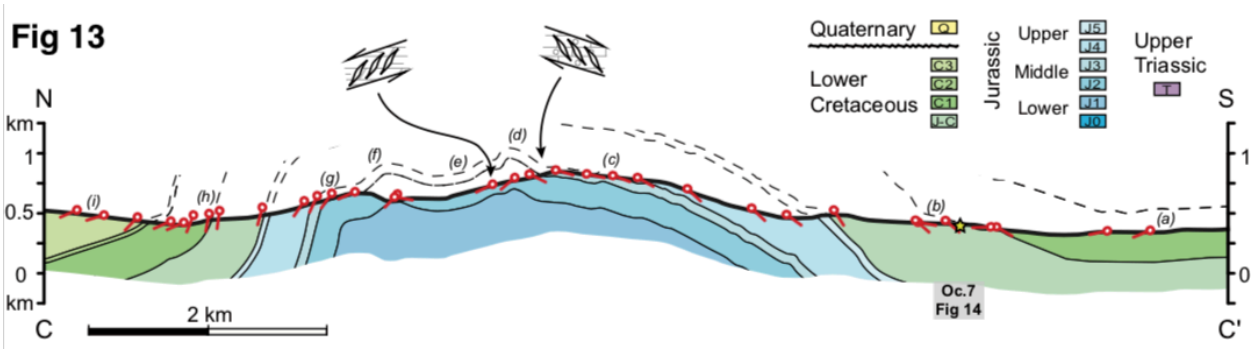

Fig. 13. Eastern profile: Cross-section C.

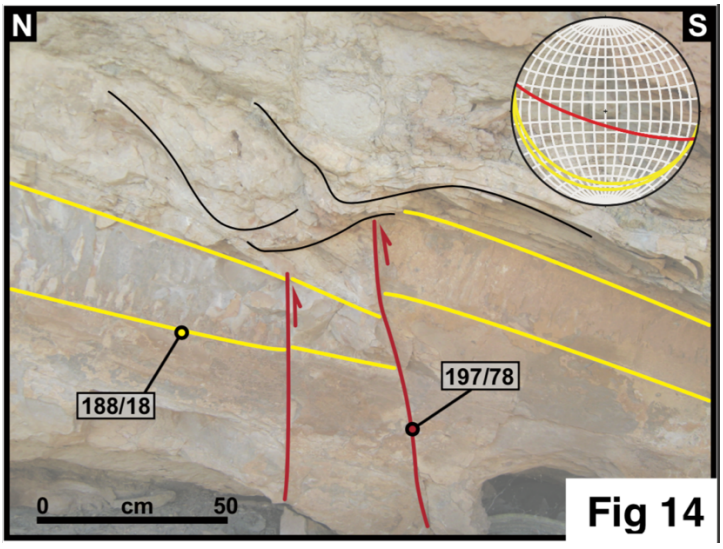

Fig. 14. Outcrop 7 (Oc.7). Inclined layers cut by synsedimentary faults. High-angle reverse faults transect a thick bank with an offset of ~20 cm. The reverse fault ends in the upper chaotic sedimentary layer that show soft sediment deformation. The timing of deformation is 146 to 137 Ma (J-C formation, lowermost Lower Cretaceous – uppermost Lower Jurassic).

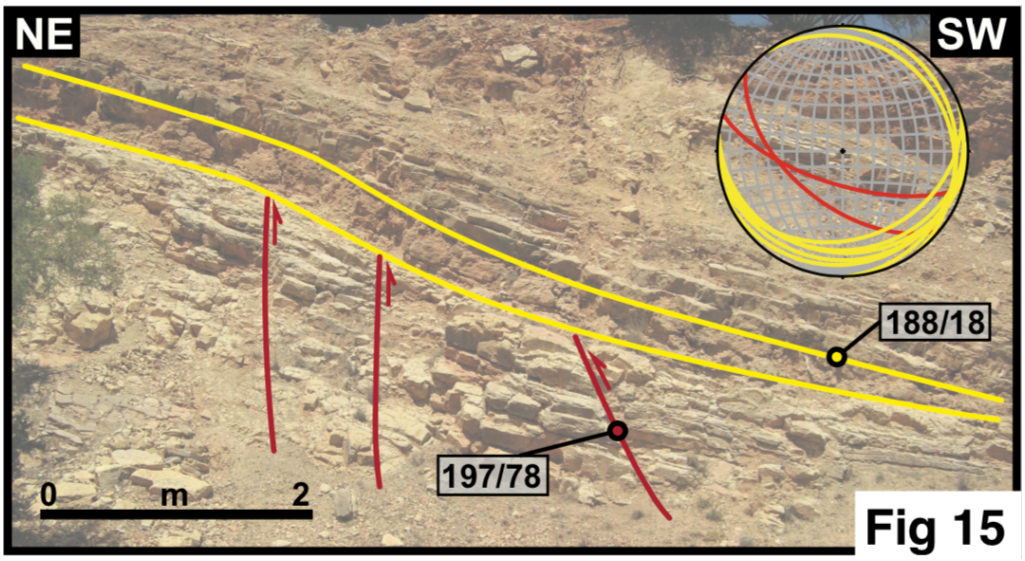

Fig. 15. Outcrop 8 (Oc.8). Approximately 30 m long wedge pinching out towards the south, overlaying faulted strata. The top to the northnortheast faults have reverse offsets of a few to tens of centimetres that do not continue in the wedge, indicating a shortening direction of SSW-NNE during the J-C formation, lowermost Lower Cretaceous – uppermost Lower Jurassic.

Outcrops farther north evidence deformation in relation to Alpine shortening. Towards the topographic high, the dip of the bedding gradually decreases from ~40° to 20° to the south, and upper Middle to middle Upper Jurassic (J3 – J4) rocks are exposed ("c"). Calcite-filled tension gashes are observed in several outcrops in and around the topographic high ("d" in Fig. 13). The veins are spaced by few cm, and show both top-to-the-north and top-to-the-south shear kinematics. The former occurs mostly to the south of the topographic high, and the latter is observed mainly to the north of the topographic high. Northwards, along a ~500 m sector, the beds are subhorizontal gently dipping to the north ("e"). Approximately 1 km farther north, beds dip to the south for ~100 m before dipping north again ("f") and lower Middle Jurassic (J2) rocks are exposed. In the second topographic high, where the second hinge plane of the anticline intersects the topography, the orientation of the bedding is 65° to the north ("g"). Between the second topographic high and the valley north of the Jbel Amsittene Anticline, successive upper Middle Jurassic (J3) to lower Lower Cretaceous (C1) strata are exposed steeply dipping north (60-80°) ("h"). North of the valley, Lower Cretaceous (C1 to C3) strata are exposed dipping ~10 to 20° northwards ("i").

3.4 Eastern sectors of the Jbel Amsittene and lateral variations

Other relevant structural observations were found eastwards of the above-described sections. The most relevant for the scope of this study outcrops ~5 km to the east of cross-section C, in the lowermost Cretaceous (J-C) limestones (Oc.8; Figs 4 and 15). This outcrop depicts a series of high angle reverse faults dipping SSW below a ~30 m long wedge that pinches out towards the S. The top-to-the-north faults show reverse offsets of few to tens of centimeters and slickenlines indicating SSW-NNE shortening direction. The fault tips lay within the overlying syn-tectonic strata, and indicate active shortening during the lowermost Cretaceous.

We reconstruct two other sections further east, where strain is more limited (Fig. 16). These sections are relatively similar in overall structure and geometry and change relevantly, albeit continuously, along the strike of the anticline. The eastern profiles depict a open and asymmetrical anticline with a gentle north vergence. In the eastern profiles, (i) the southern limb dips gently and persistently south, (ii) salt deformation is not noticeable, neither in the hinge nor elsewhere, and (iii) the northern limb shows north dips with no overturned strata. The anticline shows a well-confined hinge and its flanks dip more gently than their western continuations. Small-scale structures are rare and more open in character. The layers along the limbs alternate sectors of constant dip with others where they vary progressively. The western profiles present a tight structure and a clear north vergence. In the western profiles, (i) the southern limb of the anticline dips south, from gently to steep, with local dips to the north, (ii) distortion by diapirism is limited to near the hinge where the salt is outcropping, and (iii) the northern limb is frequently overturned and partly covered by Quaternary deposits. The western profiles show a topographic crest characterized by a north tête-plongeante geometry. Strain markers are numerous and strata often show relevant changes in dip direction over short horizontal distances.

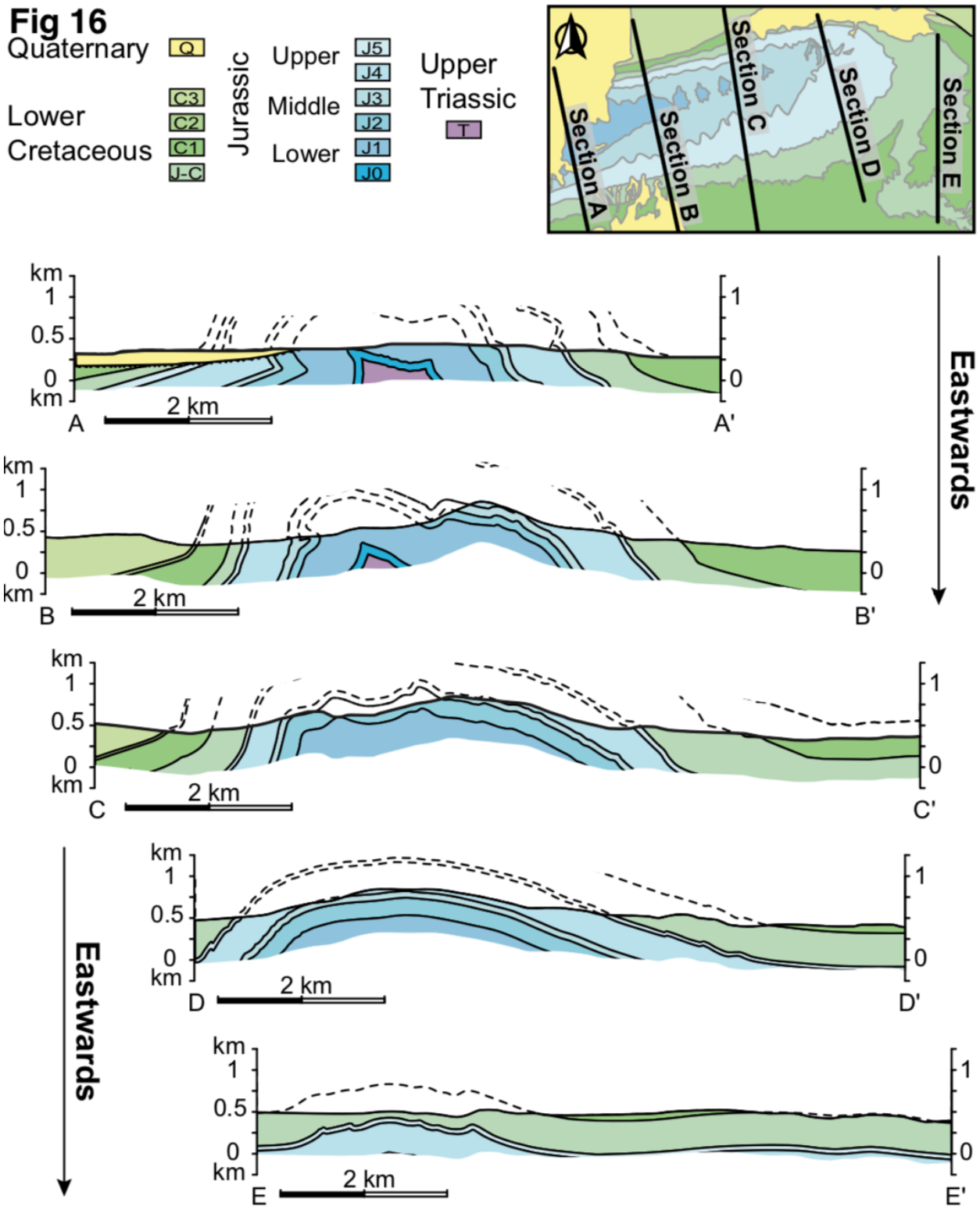

316

317 **Fig. 16.** Geological profiles from west to east.

3.5 Thickness changes along the Jbel Amsittene

To obtain thickness variations in the Jurassic formation, we put forward a 3D thickness model integrating remote sensing (horizon mapping) and structural data (dip data, geological cross sections) (Fig. 17). We use a "3 point-solver" plug-in for Google Earth™ to derive bed attitude from their contact with topography at three or more points (Bennison and Moseley 2003) and collect large-scale dip data at various locations around the anticline. We mapped horizons on DEM-coupled satellite images (Google Earth Pro™) to obtain spatial coordinates of well-exposed geological contacts, identified by the georeferenced geological map of Choubert (1965) and color changes in the imagery. We used the mapped horizons and the large-scale (tens of meters) dip data in geological cross-sections to derive a 3D model of continuous stratigraphic surfaces using *Gocad*'s *StructuralLab* tool. We then obtained true thickness maps by means of the *kine3d-1* tool that we extracted in the vicinity of mapped horizons using *Matlab*. Model resolution suggests a precision of ~20 m and hence lies below the thinnest stratigraphic units within the study area.

Lateral thickness maps reveal an along-strike change in the thickness of Jurassic rocks. Thickness variations in Figure 17 comprise the Lower Jurassic (J0, J1), Middle Jurassic (J2, J3), Upper Jurassic (J4, J5) along a clockwise profile from the northwestern to the southwestern fold flanks. Thickness decrease from the overturned northern flank, where maximum thicknesses exits, towards the east, with substantial decreases occurring at the point where the fold limbs change into NNW dipping beds. All formations follow this trend, that becomes less significant towards the Upper Jurassic (J4, J5). It is worth noticing, however, that modeling is less precise in overturned layers. In the southern limbs, towards the west, thicknesses in all formations increase progressively, albeit remaining below thicknesses of the northern limb (Fig. 17). Generally, thicknesses are never constant along strike for >5 km. Thickness at the eastern side yields around 40 to 50 m in the J3 and 140 m and 80 m for the J4, respectively. Sediments increase in thicknesses towards the southern limbs, yielding 140 to 200 m for the J3. This corresponds to a thickness increase of ~70- 75%. The J4a (Oxfordian) strongly increases from around 140 m to more than 300 m.

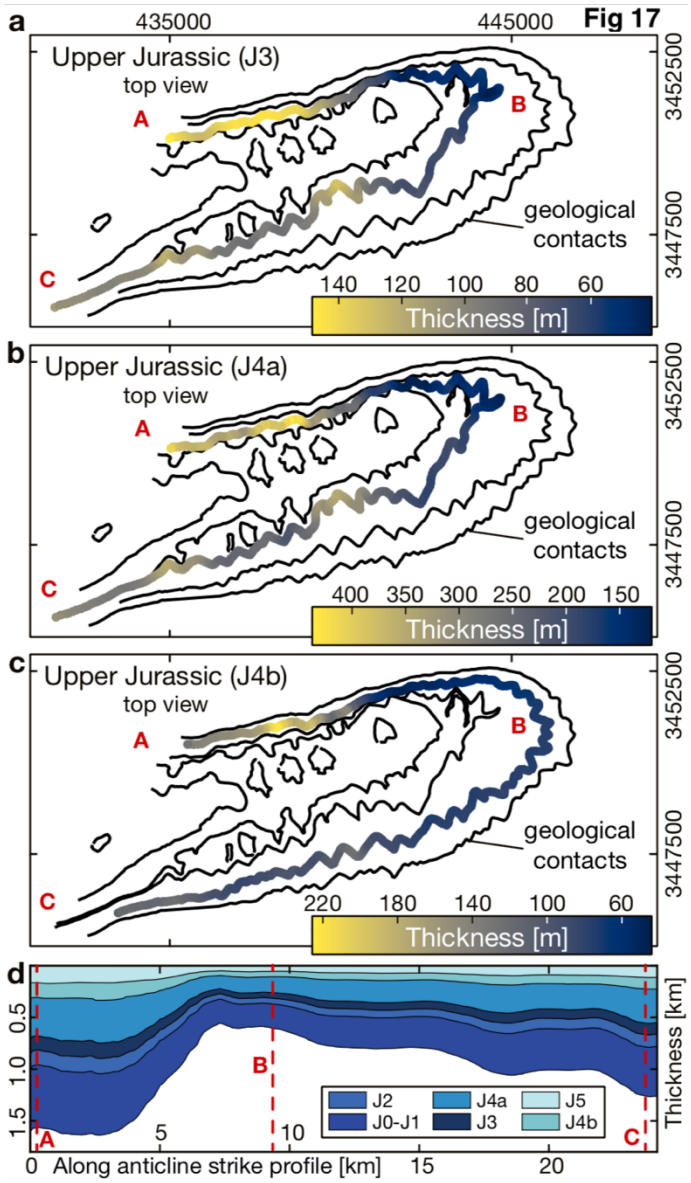

343 **Fig. 17. a/b/c** Model of thickness variations along contour likes of three Upper Jurassic sequences. **d** Modelled thickness
344 variations of Jurassic rocks in a clockwise profile from the northwestern to the southwestern flank of the anticline.

345 We derive thickness in the upper Upper Jurassic - Lower Cretaceous sedimentary units (J-C, C1, and
346 C2) from the attitude of beds within the units and along their contacts. We use this input to infer the planes
347 of contact between the sedimentary units and calculate unit thicknesses by measuring orthogonally the
348 distance between contacts. Although this approach is less accurate and lacks the along-strike coverage of
349 the aforementioned thickness model, it provides a valid first-order signal on the across-strike variation of
350 sedimentary thickness. These upper Upper Jurassic - Lower Cretaceous units (J-C, C1, and C2) decrease in

thickness northwards across the strike of the Jbel Amsittene Anticline (Table II). As seen in cross-sections A and B (Figs. 5 and 11), formations J-C and C1 are up to ~350 m thinner in the northern flank with respect to the southern flank of the anticline (Table II). These values represent a minimum estimate, given that the upper boundary of C1 is on occasion outside the limits of our study area. Although unconstrained, our observations suggests that sedimentary thickness changes also affect also C2, and that no thickness changes affect the Lower Cretaceous C3 formation. These thickness variations are less obvious towards the east (Fig. 16).

	Formation J-C		Formation C1	
	N flank	S flank	N flank	S flank
Cross-section B	150m	500m	350m	500m
Cross-section C	400m	650m	350m	450m

Table II. Thickness changes between the northern and the southern flank of the Jbel Amsittene Anticline for formations J-C and C1.

4 Discussion

4.1 Key characteristics of the Jbel Amsittene Anticline

The Jbel Amsittene Anticline has a limited lateral extent and shows geometry changes along strike. In the west, the anticline manifests as a box anticline with a gentle north vergence within a broader area of deformation. The anticline continues west into the offshore, but seismic data show no folding ~10 km westwards off the coastline (Hafid, 2006). A tight tête-plongeante that the anticline has in the west smoothens and widens into an open fold (up to 40 km) and dims away eastward, as the anticline axial plane dips south and the fold axis plunges eastwards. Given the southward dip of the anticline axial plane, the oldest rocks at the anticline core locate to the north of the topographic high. Similarly, the eastward plunge of the anticline axis results in older rocks been exposed in the west.

Thickness variations have different trends in Jurassic and Early Cretaceous units. Jurassic units show a clear signal of westward decreasing thicknesses along strike (Fig. 17). Sharp thickness variations of up to

373 900 m occur between the northern flank and the eastern termination of the anticline, while thickness
374 variations of ~600 m take place between the latter and the southern flank. A second-order signal across the
375 anticline strike portrays a decrease in thicknesses towards the southern flank (Fig. 17). Uppermost Jurassic
376 and Early Cretaceous units show the opposite trend. Sedimentary units J-C and C1 have thickness that
377 decrease in up to 500 m northwards across the strike of the anticline, in turn decreasing eastwards some
378 150 m over short horizontal distances (Table II). Whereas thickness changes in Jurassic units seem
379 unrelated with to a tectonic event, the latter units may relate with changes in shortening rates (see below).

380 Differential strain distribution along the anticline strike can be inferred for modern and antecedent
381 forms of the Jbel Amsittene Anticline. We derive these along-strike strain changes from variations in the
382 amount of shortening along the present anticline strike and from the number and size of outcrop-scale syn-
383 sedimentary structures in the Upper Jurassic – lower Lower Cretaceous (J-C) formation (Table III). The
384 western profile presents shortening values of ~1,6 km over a measured length of ~7,6 km, i.e., ~21%
385 shortening. This shortening value remains almost constant in the central profile (~20 %), and decreases in
386 the eastern profile (14,5 %). Farther east, in the easternmost section, we measured 0,2 km of shortening
387 over a length of ~4,3 km, i.e. ~4,5 % shortening (Table III). Thus, strain decays along the Jbel Amsittene
388 Anticline strike from its center to the east. Although most deformation and probably the observed eastward
389 decay in shortening along the anticline strike relates to structure tightening during Alpine times, we infer a
390 similar trend for the syn-depositional structures in the Upper Jurassic – lower Lower Cretaceous (J-C)
391 formation. Most of such syn-depositional structures appear in the west of the anticline and are absent in
392 rocks of the same age in the east and in the upper Lower Cretaceous (C3) rocks exposed in the northern
393 part of the study area. This suggest that shortening that decreased eastwards resulted the growth of an
394 anticline, albeit more open than at present, by the end of the Lower Cretaceous (C3).

	Deformed length (km)	Shortening (km)
Cross-section A	7,6	1,6
Cross-section B	9,5	2,1
Cross-section C	10,3	1,5
Cross-section D	9,1	0,6
Cross-section E	4,3	0,2

395

396 **Table III.** Decrease in amount of shortening to the east.

397 Syn-sedimentary deformation is common in outcrops of the uppermost Upper Jurassic-lowermost
398 Lower Cretaceous limestones (J-C). Syn-sedimentary strain in these outcrops is expressed as neptunian
399 dykes, fault-related folds and reverse faults affecting soft sediment (Figs. 7, 8, 14 & 15). Overall top-to-
400 the-north steep reverse faults with tips that offset soft sediments by few to tens of centimeters (Figs. 8, 14
401 & 15) suggest N-S to NNE-SSW shortening. This observation can be potentially coupled with striae in
402 nearby conjugate fault sets indicating NNW-SSE to NNE-SSW maximum horizontal stresses (Fig. 6).
403 Similar evidence of syn-sedimentary shortening during deposition of the J-C unit can be found along the
404 anticline strike. However, regional layer dips of the unit vary greatly (between approximately 30° and 80°),
405 and evidence in other outcrops, such as the tête-plongeante or the overturned strata, are clear indications of
406 later shortening of the Jbel Amsittene. Taken together, our data suggest that shortening during the early
407 post-rift phase of the Central Atlantic initiated anticline growth of the Jbel Amsittene, and that the anticline
408 further developed and tightened, presumably during the Alpine orogeny.

409 ## 4.2 Models for the evolution the Jbel Amsittene Anticline

410 We put forward two potential models for the evolution of the Jbel Amsittene Anticline in Mesozoic times.
411 We then discuss, on the basis of the evidence presented in this contribution, our preferred model for such
412 initial anticline development, which was enhanced and partly overprinted in the Cenozoic. Comparative,
413 detailed structural studies inclusive of similar onshore anticlines in the area are required to confidently
414 discriminate among evolutionary models of the Jbel Amsittene anticline, and elucidate the underlying
415 growth mechanism for equivalent structures in the Moroccan margin. Discrimination among different
416 models in turn would have implications on the geodynamic causes controlling the anomalous vertical
417 motions during the early post-rift phase along the African margin.

418 In a first scenario, we assume that the Triassic salt at the core of the present anticline is the driving
419 force leading anticline growth already during the Early to Middle Jurassic. Halokinesis and salt tectonics

420 are well expressed in the area (Hafid et al. 2006; Hafid 2000) and proposed to happen during this period in
421 the Central High-Atlas (Saura et al. 2013). Although extensive diapirism exist offshore Morocco, no clear
422 interpretation on timing and mechanism of salt mobilisation is available, and thus may occur in relation to
423 different mechanisms than in the onshore (Neumaier et al. 2016). Still, vertical movements (Stets 1992;
424 Bertotti and Gouiza 2012; Gouiza et al. 2017) could be linked to anticline fold growth and salt tectonics,
425 such that a gravitational load is applied by the uplift of the High Atlas and a subsiding continental margin,
426 creating a hydraulic head and consequent salt activation (Kluge 2016). The presence of salt in the anticline
427 core and Jurassic thickness variations along the anticline that do not relate to the present structure are
428 potential indicators for such salt tectonics scenario, although further evidence from nearby anticlines, such
429 as the Imouzzer anticline, need to be found.

430 In a second scenario, the Jbel Amsittene Anticline initially developed by horizontal shortening in
431 the latest Jurassic and earliest Cretaceous. Shortening during the Late Jurassic-Early Cretaceous marks an
432 initial period of contraction and folding during the early post-rift phase that leads to the syn-tectonic growth
433 of sedimentary wedges at anticline and outcrop scales (Figs. 8 & 11). Shortening started during latest
434 Jurassic – earliest Cretaceous (J-C), continued during the deposition of the Lower Cretaceous unit (C1),
435 and ended before the deposition of C3 unit. During this time, the Jbel Amsittene developed as open anticline
436 that was probably asymmetrical along strike. The Triassic salt functions as a weak detachment facilitating
437 accommodation of horizontal stresses leading to the partial inversion of pre-existing structures and initial
438 anticline growth before Cenozoic tectonics (Hafid et al. 2006; Tari et al. 2003; Hafid 2006).

439 Evidence reported here favours early post-rift growth of the Jbel Amsittene by shortening. The
440 shortening tectonics scenario is consistent with present of syn-sedimentary structures in the J-C unit and
441 the existence of structures with clear vergence tens of meters away from the outcropping salt and well as
442 with the limited strain (Figs. 7 to 10) near its contact. We similarly consider the lack of coherency in trend
443 or scale of the salt with the overall anticline structure are also indicators of absence of halokinesis in the
444 Jbel Amsittene during early post-rift of the Central Atlantic. Our observations imply that Triassic salts were

445 mobilised during compression driven by horizontal tectonic forces, and the growth of associated structures
446 occurs in relation to a blind thrusts rooted in the salts. The tête-plongeante structure towards the west and
447 overturned layers at some sites indicate further shortening and anticline tightening during Alpine times.
448 These geometries and their consistent changes along strike (Figs. 5, 11, 13 & 16) favour vertical anticline
449 growth during two overprinting phases of shortening acting roughly in the N-S direction over growth by
450 disruptive diapiric rise.

451 The ENE-WSW strike of the Jbel Amsittene Anticline is parallel to the strike of the major structures
452 bounding the High Atlas belt (Fig. 2). These structures activated under a transtensional regime during the
453 Triassic-Early Jurassic rifting, and defined several pull-apart basins where grabens and half-grabens,
454 bounded by N- to NE-trending normal faults, were filled by terrigenous and evaporitic series (Piqué et al.
455 2002; Laville et al. 2004; Frizon de Lamotte 2005). In our attempt to reconstruct the evolution of the Jbel
456 Amsittene through time, we hypothesize that the Jbel Amsittene Anticline formed in strata overlying a
457 previous graben structure, which was bounded by an E-dipping normal fault to the east and an E-W
458 transform fault to the north (Fig. 18). The presence and relative accommodation space expected from both
459 these pre-existing structures could explain increasing Jurassic thicknesses westwards and northwards (Fig.
460 17), along and across anticline strike respectively. We interpret the upwards decreasing thickness in Upper
461 Jurassic units (Fig. 17) as an indication that the aforementioned faults were nearly sealed by the end of the
462 Late Jurassic. Subsequent Late Jurassic-Early Cretaceous folding of the Jbel Amsittene Anticline may have
463 occurred by reactivation of the E-W structure as a blind thrust. This would result in thickness that increase
464 towards the hanging-wall, i.e. southwards across the anticline and are thus opposite in trend with regards
465 to those in the Jurassic units (Table II). Such blind thrust would be rooted in Triassic evaporites that act as
466 a weak decollement layer between the basement and the overlying Mesozoic basin infill (Fig. 18).
467 Therefore, most of the strain was localised in the depocentre of the Triassic salt found underneath the
468 western part of the Jbel Amsittene and wedging out towards the east. This is coherent with eastwards
469 decreasing strain observed for both the early post-rift and the Alpine shortening phases.

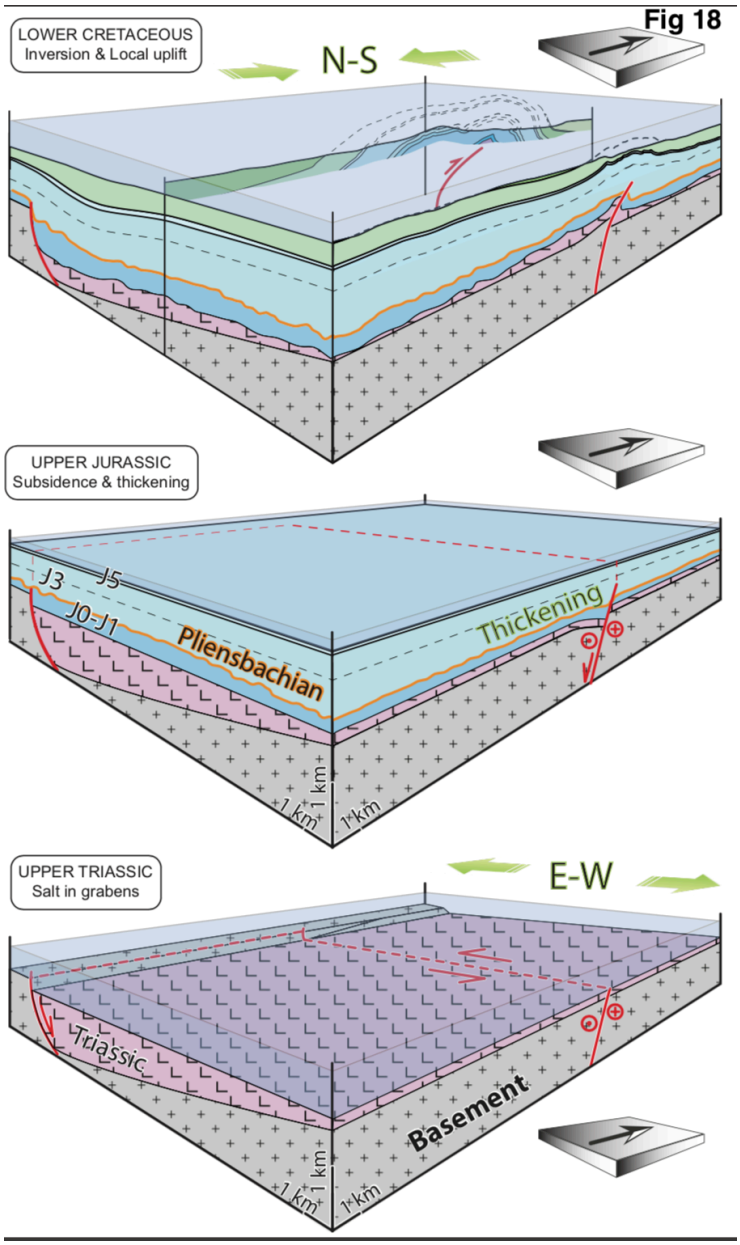

Fig. 18. Proposed evolutionary model for the Jbel Amsittene Anticline.

4.3 Regional shortening during anticline growth

Observations from other areas within and nearby the Essaouira Basin suggest that the other salt structures present in the margin, may not have originally developed entirely during the Tertiary contraction. This is the case of the Tidsi Anticline and the Imi n'Tanout wedge in the Essaouira Basin, and the Dadès Valley in

476 the Ouarzazate Basin. These structures may have formed similarly to the Jbel Amsittene Anticline, i.e.
477 during an early post-rift shortening phase that reactivated inherited structures in assistance of the Triassic
478 evaporitic rocks (Fig. 17). However, truncation of the basalt horizons by the Pliensbachian unconformity
479 within certain structures also suggest the presence of earlier salt growth (Hafid et al. 2006).

480 The Tidsi Anticline, north of the Jbel Amsittene Anticline, was also thought to result from salt
481 diapirism during the Late Cretaceous; the main arguments were the presence of growth strata documented
482 in the Upper Cretaceous rocks coupled with the absence of tectonic indicators associated with these growth
483 features (Amrhar 1995; Hafid 2006). While the relevance of diapirism in controlling the growth of the Tidsi
484 Anticline during Late Cretaceous time is not unlikely, other older structures are observed in the area which
485 document the existence of Early Cretaceous tectonic deformations hitherto neglected (Bertotti and Gouiza
486 2012). The best structures are visible along a >1 km long cliff in the southern part of the Tidsi Anticline
487 where Triassic to Cretaceous sediments outcrop. A clear wedge described by Lower Cretaceous rocks opens
488 southwards bounded on the southern side by steeper layers showing folded Early Lower Cretaceous beds
489 along a WNW-ESE to NW-SE axis, that is parallel to the strike of the wedge. Strata geometry points to a
490 NNE-ward vergence of the structure. Late Lower Cretaceous strata in the uppermost part of the outcrop are
491 sub-horizontal, documenting the pre-Late Cretaceous age of deformation (Bertotti and Gouiza 2012). The
492 tectonic nature of these structures is not only suggested by their overall geometry but is also proven by the
493 fold vergence towards the core of the Tidsi Anticline, which is incompatible with a halokinetic origin.

494 To the east of Jbel Amsittene, the geometry of the post-rift portion of the Imi n'Tanout wedge prior to
495 Alpine shortening was reconstructed coupling thickness measurements with structural field observations
496 (Zühlke et al. 2004; Bertotti and Gouiza 2012). The post-rift strata show a gradual increase in thickness
497 from NE to SW, reaching more than 3000 m towards the coastal areas and indicating that the Imi n'Tanout
498 wedge opened along a NNW-SSE to NW-SE trending axis. Fieldwork observations in the Imi n'Tanout
499 region reveal also the presence of two sets of shortening structures (Bertotti and Gouiza 2012). An older
500 set oriented NW-SE to WNW-ESE is documented by syn-sedimentary structures that affect Middle Jurassic

to Lower Cretaceous sediments to the south of the Imi n'Tanout line. At the outcrop-scale syn-depositional deformation is common in the Imi n'Tanout wedge and typically show folds and thrusts with a NW-SE trending axis. All these structures document Late Jurassic to Early Cretaceous NE-SW shortening approximately perpendicular to the axis of the Imi n'Tanout wedge suggesting that they developed within the same deformation regime. The younger set, oriented E-W to WSW-ENE, is found mainly in the Cretaceous sediments to the N of the Imi n'Tanout line and characterized by symmetrical to vergent folds. This set is conformal to the large-scale folds in the northern part of the Essaouira Basin that are related to the inversion of the Atlas system.

In the Ouarzazate foreland basin, located southeast of the Essaouira Basin and south of the central High Atlas (Fig. 1), strong evidences indicate a pre-Atlasic shortening event (Benvenuti et al. 2017). Observations from the Dadès Valley in the eastern Ouarzazate Basin indicate syn-tectonic angular and progressive unconformities within the Middle Jurassic to Lower Cretaceous stratigraphic units (Benvenuti et al. 2017). In addition, syn-sedimentary tectonic structures were also documented and suggest a first Middle Jurassic-Early Cretaceous NNE-SSW to NNW-SSE shortening and a later E-W shortening during the Late Cretaceous (Benvenuti et al. 2017).

4.4 Tectonic setting during anticline growth

The timing of the contractional structures observed in the Essaouira Basin coincides with major rearrangements in plate motions related to the opening of the South and North Atlantic Ocean. In fact, continental separation and accretion of oceanic crust in the South Atlantic (Torsvik et al. 2009), between SW Africa and South America, and in the North Atlantic (Knott et al. 1993; Tucholke et al. 2007), between North America and Eurasia, started in the Aptian-Albian time. The resulting counterclockwise rotation of Africa and the southward drifting of Iberia led to N-S compressive stresses within the African plate. At the same time, the ongoing oceanic accretion and mid-Atlantic ridge push in the Central Atlantic resulted in E-W compressive stresses. We believe that Late Jurassic-Early Cretaceous shortening in the Essaouira Basin

was driven by these N-S and E-W compressive stresses that reactivated the E-W and N-S syn-rift structures alike and initiated the subsequent salt movements onshore and offshore the Moroccan rifted margin (Hafid et al. 2006; Hafid 2000, 2006; Tari et al. 2003).

On the other hand, the spatial and temporal relation between these contractional structures and the regional uplift event that affected the NW African margin may suggest a common genetic process. Mantle processes like small-scale convection cells acting at the base of the mantle lithosphere cannot fully explain km-scale uplift of the crust during the early post-rift time their own, but if combined with intraplate stresses, the resulting uplift may be enhanced (Gouiza 2011).

5 Conclusion

We present structural and stratigraphic evidences demonstrating that the Jbel Amsittene is a N-verging fault-related anticline with its detachment plane in the Late Triassic evaporites. We have shown that the Jbel Amsittene (i) largely lack structures related to diapiric rise (only observable few hundred meters away from the outcropping evaporites), although recent literature promotes this mechanism; (ii) is an asymmetrical fault-propagation anticline with a steeply dipping northern, locally overturned, flank and a shallowly dipping southern flank; and (iii) underwent syn-sedimentary shortening during Late Jurassic-Early Cretaceous times.

The development of Jbel Amsittene was mainly driven by compressional tectonics and only partially the result of salt tectonics. The anticline formed during NNW-SSE shortening that initiated by the end of the Late Jurassic, potentially in the western part of the structure. Shortening resulted in syn-tectonic wedges at anticline and outcrop scale, in Late Jurassic and Early Cretaceous strata, while the effect of salt diapirism was restricted to a local area around the core of the anticline. The later inversion of the Atlas system in the Late Cretaceous and the Neogene caused the tightening of the anticline. Being one of many contemporaneous contractional structures reported in the Essaouira Basin and nearby basins linked to km-

548 scale Middle Jurassic to Early Cretaceous exhumation event along the entire NW African margin,
549 observations in the Jbel Amsittene Anticline suggest a tectonic evolution driven by intraplate stresses and
550 deep mantle processes.

551

552 References

553 Amrhar M (1995) Évolution structurale du Haut Atlas occidental dans le cadre de l'ouverture de
554 l'Atlantique centrale et de la collision Afrique--Europe: Structure, instabilités tectoniques et
555 magmatisme. Thèse Doct. Etat, Univ. Cadi Ayyad, Marrakech

556 Bennison G, Moseley K (2003) An Introduction to Geological Structures and Maps 7ed

557 Benvenuti M, Moratti G, Algouti A (2017) Stratigraphic and structural revision of the Upper Mesozoic
558 succession of the Dadès valley, eastern Ouarzazate Basin (Morocco). J Afr Earth Sci 135:54–71

559 Bertotti G, Gouiza M (2012) Post-rift vertical movements and horizontal deformations in the eastern
560 margin of the Central Atlantic: Middle Jurassic to Early Cretaceous evolution of Morocco. Int J
561 Earth Sci 101:2151–2165

562 Bonow JM, Japsen P, Green PF, et al (2009) Post-rift landscape development of north-east Brazil.
563 Geological Survey of Denmark and Greenland Bulletin 17:81–84

564 Charton R, Bertotti G, Arantegui A, Bulot L (2018) The Sidi Ifni transect across the rifted margin of
565 Morocco (Central Atlantic): Vertical movements constrained by low-temperature thermochronology.
566 J Afr Earth Sci 141:22–32

567 Duffaud F, Brun L, Plauchut B (1966) Le bassin du Sud-Ouest marocain. Bassins sédimentaires du
568 littoral Africain Publ Assoc Serv Géol Afric 1:5–26

569 Ellouz N, Patriat M, Gaulier J-M, et al (2003) From rifting to Alpine inversion: Mesozoic and Cenozoic
570 subsidence history of some Moroccan basins. Sediment Geol 156:185–212

571 Frizon de Lamotte D (2005) About the Cenozoic inversion of the Atlas domain in North Africa. C R
572 Geosci 337:475–476

573 Frizon de Lamotte D, Andrieux J, Guezou JC (1991) Cinematique des chevauchements neogenes dans
574 l'Arc betico-rifain; discussion sur les modeles geodynamiques. Bull Soc Geol Fr 162:611–626

575 Frizon de Lamotte D, Saint Bezar B, Bracène R, Mercier E (2000) The two main steps of the Atlas
576 building and geodynamics of the western Mediterranean. Tectonics 19:740–761

577 Frizon de Lamotte D, Zizi M, Missenard Y, et al (2008) The Atlas System. In: Michard A, Saddiqi O,
578 Chalouan A, de Lamotte DF (eds) Continental Evolution: The Geology of Morocco. Springer
579 Nature, Berlin Heidelberg, pp 133–202

580 Ghorbal B (2009) Mesozoic to Quaternary thermo-tectonic evolution of Morocco (NW Africa). Vrije
581 Universiteit Amsterdam

582 Ghorbal B, Bertotti G, Foeken J, Andriessen P (2008) Unexpected Jurassic to Neogene vertical
583 movements in "stable" parts of NW Africa revealed by low temperature geochronology. Terra Nova
584 20:355–363

585 Gouiza M (2011) Mesozoic Source-to-Sink Systems in NW Africa:: Geology of vertical movements
586 during the birth and growth of the Moroccan rifted margin. Vrije Universiteit Amsterdam

587 Gouiza M, Bertotti G, Andriessen PAM Mesozoic and Cenozoic thermal history of the western Reguibat
588 Shield (West African Craton). Terra Nova. doi: 10.1111/ter.12318

589 Gouiza M, Charton R, Bertotti G, et al (2017) Post-Variscan evolution of the Anti-Atlas belt of Morocco
590 constrained from low-temperature geochronology. Int J Earth Sci 106:593–616

591 Hafid M (2000) Triassic–early Liassic extensional systems and their Tertiary inversion, Essaouira Basin
592 (Morocco). Mar Pet Geol 17:409–429

593 Hafid M (2006) Styles structuraux du Haut Atlas de Cap Tafelney et de la partie septentrionale du Haut
594 Atlas occidental: tectonique salifère et relation entre l'Atlas et l'Atlantique. Notes Mém Serv Géol
595 Maroc 465:172

596 Hafid M, Zizi M, Bally AW, Ait Salem A (2006) Structural styles of the western onshore and offshore
597 termination of the High Atlas, Morocco. C R Geosci 338:50–64

598 Jaïdi S, Bencheqroun A, Diouri M (1970) Carte Géologique du Maroc 1:100 000, Feuille Tamanar. Not
599 Mém Serv Géol Maroc 201:

600 Japsen P, Bonow JM, Green PF, et al (2006) Elevated, passive continental margins: Long-term highs or
601 Neogene uplifts? New evidence from West Greenland. Earth Planet Sci Lett 248:330–339

602 Japsen P, Bonow JM, Green PF, et al (2009) Formation, uplift and dissection of planation surfaces at
603 passive continental margins – a new approach. Earth Surf Processes Landforms 34:683–699

604 Japsen P, Chalmers JA (2000) Neogene uplift and tectonics around the North Atlantic: overview. Glob
605 Planet Change 24:165–173

606 Klitgord KD, Schouten H (1986) Plate kinematics of the central Atlantic. The Geology of North America
607 1000:351–378

608 Kluge C (2016) A Structural Modeling Approach on Timing & Evolution of Mesozoic Anticlines in the
609 Western High Atlas, Morocco

610 Knott SD, Burchell MT, Jolley EJ, Fraser AJ (1993) Mesozoic to Cenozoic plate reconstructions of the
611 North Atlantic and hydrocarbon plays of the Atlantic margins. In: Petroleum Geology of Northwest
612 Europe: Proceedings of the 4th Conference. Geological Society of London, pp 953–974

613 Laville E, Piqué A (1992) Jurassic penetrative deformation and Cenozoic uplift in the Central High Atlas
614 (Morocco): A tectonic model. structural and orogenic inversions. Geol Rundsch 81:157–170

615 Laville E, Pique A, Amrhar M, Charroud M (2004) A restatement of the Mesozoic Atlasic Rifting
616 (Morocco). J Afr Earth Sci 38:145–153

617 Leprêtre R, Missenard Y, Barbarand J, et al (2015) Postrift history of the eastern central Atlantic passive
618 margin: Insights from the Saharan region of South Morocco. J Geophys Res [Solid Earth]
619 120:2014JB011549

620 Le Roy P, Piqué A (2001) Triassic–Liassic Western Moroccan synrift basins in relation to the Central
621 Atlantic opening. Mar Geol 172:359–381

622 Malusà MG, Polino R, Feroni AC, et al (2007) Post-Variscan tectonics in eastern Anti-Atlas (Morocco).
623 Terra Nova 19:481–489

624 Medina F (1995) Syn- and postrift evolution of the El Jadida – Agadir basin (Morocco): constraints for
625 the rifting models of the central Atlantic. Can J Earth Sci 32:1273–1291

626 Neumaier M, Back S, Littke R, et al (2016) Late Cretaceous to Cenozoic geodynamic evolution of the
627 Atlantic margin offshore Essaouira (Morocco). Basin Res 28:712–730

628 Oukassou M, Saddiqi O, Barbarand J, et al (2013) Post-Variscan exhumation of the Central Anti-Atlas
629 (Morocco) constrained by zircon and apatite fission-track thermochronology. Terra Nova 25:151–
630 159

631 Peulvast J-P, Claudino Sales V, Bétard F, Gunnell Y (2008) Low post-Cenomanian denudation depths
632 across the Brazilian Northeast: Implications for long-term landscape evolution at a transform
633 continental margin. Glob Planet Change 62:39–60

634 Piqué A, Le Roy P, Amrhar M (1998) Transtensive synsedimentary tectonics associated with ocean
635 opening: the Essaouira–Agadir segment of the Moroccan Atlantic margin. J Geol Soc London
636 155:913–928

637 Piqué A, Tricart P, Guiraud R, et al (2002) The Mesozoic-Cenozoic Atlas belt (North Africa): an
638 overview. Geodin Acta 15:185–208

639 Ruiz G, Sebti S, Negro F, et al (2011) From central Atlantic continental rift to Neogene uplift--western
640 Anti-Atlas (Morocco). Terra Nova 23:35–41

641 Saddiqi O, El Haimer F-Z, Michard A, et al (2009) Apatite fission-track analyses on basement granites
642 from south-western Meseta, Morocco: Paleogeographic implications and interpretation of AFT age
643 discrepancies. Tectonophysics 475:29–37

644 Sahabi M, Aslanian D, Olivet J-L (2004) Un nouveau point de départ pour l'histoire de l'Atlantique
645 central. C R Geosci 336:1041–1052

646 Saura E, Vergés J, Martín-Martín JD, et al (2013) Syn- to post-rift diapirism and minibasins of the
647 Central High Atlas (Morocco): the changing face of a mountain belt. J Geol Soc London 171:97–105

648 Seguret M (1972) Étude tectonique des nappes et séries décollées de la partie centrale des Pyrénées.
649 Thesis. Science Univ. Montpellier

650 Sehrt M (2014) Variscan to Neogene long-term landscape evolution at the Moroccan passive continental
651 margin (Tarfaya Basin and western Anti-Atlas). Heidelberg

652 Stets J (1992) Mid-Jurassic events in the Western High Atlas (Morocco). Geol Rundsch 81:69–84

653 Tari G, Molnar J, Ashton P (2003) Examples of salt tectonics from West Africa: a comparative approach.

654 Geological Society, London, Special Publications 207:85–104

655 Teixell A, Arboleya M-L, Julivert M, Charroud M (2003) Tectonic shortening and topography in the
656 central High Atlas (Morocco). Tectonics 22:1051

657 Torsvik TH, Rousse S, Labails C, Smethurst MA (2009) A new scheme for the opening of the South
658 Atlantic Ocean and the dissection of an Aptian salt basin. Geophys J Int 177:1315–1333

659 Tucholke BE, Sawyer DS, Sibuet J-C (2007) Breakup of the Newfoundland–Iberia rift. Geological
660 Society, London, Special Publications 282:9–46

661 Zühlke R, Bouaouda M-S, Ouajhain B, et al (2004) Quantitative Meso-/Cenozoic development of the
662 eastern Central Atlantic continental shelf, western High Atlas, Morocco. Mar Pet Geol 21:225–276

663